

# Amplitude squeezing in a Mach-Zehnder fiber interferometer: Numerical analysis of experiments with microstructure fiber

Marco Fiorentino, Jay E. Sharping, and Prem Kumar

*Center for Photonic Communication and Computing  
ECE Department, Northwestern University, 2145 Sheridan Rd.  
Evanston, IL 60208, USA  
mfiore@ece.northwestern.edu*

Alberto Porzio

*INFN Unitá operativa di Napoli  
Complesso Universitario di M. S. Angelo, Edificio G  
80126, Napoli, Italia*

**Abstract:** We study a Mach-Zehnder nonlinear fiber interferometer for the generation of amplitude-squeezed light. Numerical simulations of experiments with microstructure fiber are performed using linearization of the quantum nonlinear Schrödinger equation. We include in our model the effect of distributed linear losses in the fiber.

© 2002 Optical Society of America

OCIS codes: 270.6570, 060.2400

---

## References and links

1. R. M. Shelby, M. D. Levenson, S. H. Perlmutter, R. G. De Voe, and D. F. Walls, "Broad-band parametric deamplification of quantum noise in an optical fiber," *Phys. Rev. Lett.* **57**, 691 (1987).
2. M. Rosenbluh and R. M. Shelby, "Squeezed optical solitons," *Phys. Rev. Lett.* **66**, 153 (1991).
3. A. Sizmann and G. Leuchs, "The optical Kerr effect and quantum optics in fibers," in *Progress in Optics XXXIX*, E. Wolf, ed. (Elsevier Science B.V., 1999).
4. Ch. Silberhorn, P. K. Lam, O. Weiß, F. König, N. Korolkova, and G. Leuchs, "Generation of continuous variable Einstein-Podolsky-Rosen entanglement via the Kerr nonlinearity in an optical fibre," *Phys. Rev. Lett.* **86**, 4267 (2001).
5. A. Furusawa, J.L. Sorensen, S. L. Braunstein, C. A. Fuchs, H. J. Kimble, and E. S. Polzik, "Unconditional quantum teleportation," *Science* **282**, 706 (1998); S. L. Braunstein and H. J. Kimble, "Dense coding for continuous variables," *Phys. Rev. A* **61** 2302 (2000).
6. S. Schmitt, J. Ficker, M. Wolff, F. König, A. Sizmann, and G. Leuchs, "Photon-number squeezed solitons from an asymmetric fiber-optic Sagnac interferometer," *Phys. Rev. Lett.* **81**, 2446 (1998).
7. S. Spälter, M. Burk, U Ströβner, A. Sizmann, and G. Leuchs, "Propagation of quantum properties of sub-picosecond solitons in a fiber," *Opt. Express* **2**, 77 (1998).
8. D. Krylov and K. Bergman, "Amplitude-squeezed solitons from an asymmetric fiber interferometer," *Opt. Lett.* **23**, 1390 (1998).
9. D. Levandovsky, M. Vasilyev, and P. Kumar, "Amplitude squeezing of light by means of a phase-sensitive fiber parametric amplifier," *Opt. Lett.* **24**, 948 (1999)
10. M. Fiorentino, J. E. Sharping, P. Kumar, D. Levandovsky, and M. Vasilyev, "Soliton squeezing in a Mach-Zehnder fiber interferometer," *Phys. Rev. A* **64**, 031801(R) (2001).
11. M. Fiorentino, J.E. Sharping, P. Kumar, A. Porzio, and R. Windeler, "Soliton squeezing in microstructure fiber," submitted to *Opt. Lett.*
12. J. K. Ranka, R. S. Windeler, and A. J. Stentz, "Visible continuum generation in air-silica microstructure optical fibers with anomalous dispersion at 800 nm," *Opt. Lett.* **25**, 25 (2000).
13. X. Liu, C. Xu, W. H. Knox, J. K. Chandalia, B. J. Eggleton, S. G. Kosinsky, and R. S. Windeler, "Soliton self-phase shift in a short tapered air-silica microstructure fiber," *Opt. Lett.* **26**, 358 (2001).
14. J. E. Sharping, M. Fiorentino and P. Kumar, "Four wave mixing in microstructure fibers," *Opt. Lett.* **26**, 1048 (2001).

15. F. G. Omenetto, A. J. Taylor, M. D. Moores, J. Arriaga, J. C. Knight, W. J. Wadsworth, and P. St. J. Russel, "Simultaneous generation of spectrally distinct third harmonics in a photonic crystal fiber," *Opt. Lett.* **26**, 1558 (2001).
16. H. A. Haus and Y. Lai, "Quantum theory of soliton squeezing: a linearized approach," *J. Opt. Soc. Am. B* **7**, 386 (1990).
17. D. J. Kaup, "Perturbation theory for solitons in optical fibres," *Phys. Rev. A* **42**, 5689 (1990).
18. D. Levandovsky, M. Vasilyev, and P. Kumar, "Soliton squeezing in a highly transmissive loop mirror," *Opt. Lett.* **24**, 89 (1999).
19. C. R. Doerr, M. Shirasaki, and F. I. Khatri, "Simulation of pulsed squeezing in optical fiber with chromatic dispersion," *J. Opt. Soc. Am. B* , **11**, 142 (1994).
20. M. Shirasaki and H. A. Haus, "Squeezing of pulses in a nonlinear interferometer," *J. Opt. Soc. Am. B* **7**, 30 (1990).
21. G. P. Agrawal, *Nonlinear Fiber Optics*, 2nd ed. (Academic, San Diego, 1995).
22. C. Caves, "Quantum limits on noise in linear amplifiers," *Phys. Rev. D* **26**, 1817 (1982).
23. W. H. Louisell, *Quantum Statistical Properties of Radiation* (Wiley, New York, 1973).
24. P. Kumar and J. Shapiro, "Squeezed-state generation via forward degenerate four-wave mixing," *Phys. Rev. A* **30**, 1568 (1984).
25. J. H. Shapiro and L. Boivin, "Raman-noise limit on squeezing in continuous-wave four-wave mixing," *Opt. Lett.* **20**, 925 (1990).
26. M. J. Werner, "Quantum soliton generation using an interferometer," *Phys. Rev. Lett.* **81**, 4132 (1998).
27. K. Bergman, H. A. Haus, E. P. Ippen, and M. Shirasaki, "Squeezing in a fiber interferometer with a gigahertz pump," *Opt. Lett.* **19**, 290 (1994).

## 1 Introduction

The generation of squeezed radiation in optical fibers using the effects of four-wave mixing and self-phase modulation has attracted considerable attention since the pioneering work with CW [1] and pulsed light [2] (see the paper by Sizmann and Leuchs [3] for an extensive review). Recently this interest has been renewed by the possibility [4] of using fiber-generated squeezed fields to create and distribute continuous-variable entanglement for quantum-communication applications such as teleportation and dense coding [5]. Several new schemes to generate squeezed light by exploiting the Kerr nonlinearity in optical fibers have been demonstrated [2, 6, 7, 8, 9]. The most successful soliton squeezing experiments to date have employed an asymmetric Sagnac interferometer [6, 8]. The amplitude squeezing in such experiments results from the combined effect of soliton's nonlinear propagation in the fiber and its subsequent mixing with an auxiliary weak pulse at the fiber output. To obtain a high degree of noise reduction, it is crucial to control the relative amplitude and phase of the two pulses. In the Sagnac configuration [6, 8] the pulses counter propagate in the same fiber, thus preventing the control of their relative phase. Moreover, the relative amplitude between the soliton pulse and the auxiliary pulse is unchangeable once one fixes the splitting ratio of the interferometer beamsplitter.

To overcome these drawbacks we have investigated [10, 11] the setup shown in Fig. 1, wherein the Sagnac geometry is "unfolded" into a Mach-Zehnder interferometer formed between BS1 and BS2. The Mach-Zehnder geometry allows independent control of the phase and amplitude of the auxiliary pulse relative to the soliton.

In our experiments we have studied the quantum-noise reduction (QNR) in two different types of fiber. In the first set of experiments [10] we used a standard PM fiber (3M-FSPM 7811) as the nonlinear element of our Mach-Zehnder interferometer. In the second set of experiments [11] the PM fiber was replaced by a microstructure fiber (MF) fabricated by Bell Laboratories, Lucent Technologies [12]. Recent experiments have demonstrated that dramatic nonlinear effects [12, 13, 14, 15], such as four-wave mixing, third-harmonic generation, and soliton self-frequency shift, can be obtained in short lengths of such fibers. In fact, MFs combine a small core area and engineerable dispersion characteristics with single-mode behavior over a wide wavelength range. These

properties are very appealing as they allow one to build a robust and compact device for generating low-energy amplitude-squeezed solitons, thus avoiding the penalties associated with high energy of squeezed solitons in standard PM fibers. One such penalty, for example, is that the accompanying high average power prevents one from making homodyne measurements on the squeezed solitons, as the required average local-oscillator power far exceeds the saturation power of most photodetectors. Together with their advantages, however, MFs suffer from the drawback of having large distributed losses compared with conventional fibers [measured losses of  $(0.6\pm 0.2)$  dB/m, that amount to a transmittivity of about 91% for the 0.70 m long piece of fiber used in our best squeezing measurements]. In this paper we discuss the effect of such distributed losses on the obtainable QNR.

The paper is organized as follows: in section 2, we describe the numerical analysis of a Mach-Zehnder interferometer in which the nonlinear fiber is considered to be lossless. In section 3, we generalize the numerical analysis to the case of a lossy fiber. Finally section 4 is devoted to the description of our experimental setup and comparison of the data with numerical simulations.

## 2 Numerical Analysis, Lossless Fiber

To optimize the experimental QNR it is crucial that we study the dependence of the noise reduction in the Mach-Zehnder interferometer on various parameters such as the splitting ratio of the interferometer's beamsplitters and the fiber length. The analysis of such dependencies requires a model for the propagation of the pulses' quantum noise in the fiber. For pulses that are fundamental solitons (i.e., soliton number  $N = 1$ ), an analytical solution for the propagation of the quantum noise of the soliton is possible [16, 17, 18]. Such analytical solution has been applied to the analysis of squeezing experiments that employ interferometers [18]. However, when the pulses are not fundamental solitons, there is no known analytical solution for the propagation of the quantum noise of the pulses. Several works have applied numerical methods to solve this problem and such numerical solutions have been used to analyze the noise-reduction properties of asymmetric Sagnac interferometers [6, 19]. A common feature of all of these works is that the calculated noise reduction exceeds, by a sizable amount, any experimental result obtained so far. Remarkably, however, the theory seems to be able to reproduce the overall qualitative structure of the experimental data.

In this section we focus our attention on the propagation of quantum noise in a lossless fiber and then apply the results to the analysis of the Mach-Zehnder interferometer employed in our experiments [10]. We use the standard linearization approximation for solving the quantum nonlinear Schrödinger equation (NLSE) [20]

$$\frac{\partial \hat{U}}{\partial z} = i\hat{U}^\dagger \hat{U} \hat{U} + \frac{i}{2} \frac{\partial^2 \hat{U}}{\partial t^2}, \quad (1)$$

which describes the evolution of the annihilation operators  $\hat{U}$  for the envelope of the electric field in the fiber. Equation (1) is written in a retarded frame moving together with the pulse along  $z$ , which is expressed in standard normalized-length units [21]. We linearize this equation by putting

$$\hat{U} = \bar{U} + \hat{u}, \quad (2)$$

where  $\bar{U} = \langle \hat{U} \rangle$  and  $\hat{u}$  is the annihilation operator for the fluctuations, and keeping only terms up to first order in  $\hat{u}$ . Such linearization approximation is valid in the limit of fluctuations that are small compared with the mean values of the field. When substituted

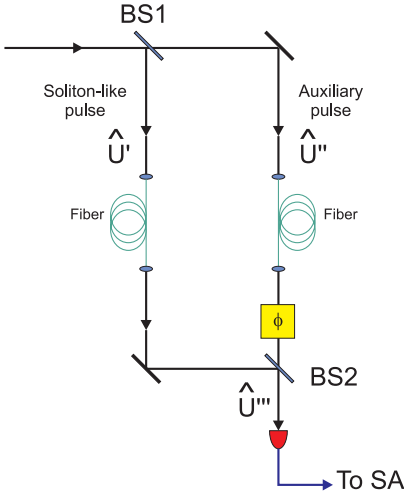


Fig. 1. Schematic model of the nonlinear fiber Mach-Zehnder interferometer. BS, beamsplitter; SA, spectrum analyzer.

in Eq. (1), equation (2) yields a pair of coupled equations: the zeroth-order expansion represents the classical NLSE, describing the evolution of the envelope  $\bar{U}$ ,

$$\frac{\partial \bar{U}}{\partial z} = i|\bar{U}|^2 \bar{U} + \frac{i}{2} \frac{\partial^2 \bar{U}}{\partial t^2}, \quad (3)$$

whereas the first-order expansion gives a linear equation for the evolution of the fluctuation operator  $\hat{u}$

$$\frac{\partial \hat{u}}{\partial z} = 2i|\bar{U}|^2 \hat{u} + i\bar{U}^2 \hat{u}^\dagger + \frac{i}{2} \frac{\partial^2 \hat{u}}{\partial t^2}. \quad (4)$$

Equation (3) can be solved numerically by discretizing the time,  $t$ , and the propagation variable,  $z$ . We use a split-step Fourier method [21], which is simple to implement with high resolution and precision. The idea underlying this method is illustrated schematically in Fig. 2 (a). The fiber is divided into small segments of length  $\Delta z$ , and an approximate solution to the equation is found by pretending that over  $\Delta z$  the nonlinearity [represented by the first term on the right side of Eq. (3)] and dispersion [represented by the second term on the right side of Eq. (3)] act independently. This approximation allows one to exactly solve each evolution step by matrix exponentiation, which can be efficiently implemented numerically. To further increase the precision of the solution, we use a symmetrized split-step method, where the dispersion is calculated at the mid plane of the segment and is preceded and followed by nonlinear propagation. Once the solution for Eq. (3) is obtained, one can solve Eq. (4) applying a discretization procedure as described by Doerr *et alii* [19]. One defines

$$\hat{u}(z, t) \equiv \sum_{j=1}^M \frac{\hat{u}_j(z)}{\sqrt{M}}, \quad (5)$$

where the pulse has been divided into  $M$  temporal slices and each time slice is treated as an independent mode of the electromagnetic field. The modes' operators evolve following Eq. (4). When Eq. (5) is substituted into Eq. (4) one obtains a set of coupled equations for  $\hat{u}$  and  $\hat{u}^\dagger$ . Without loss of generality one can express the mode  $u_j$  in  $z$  as [19]

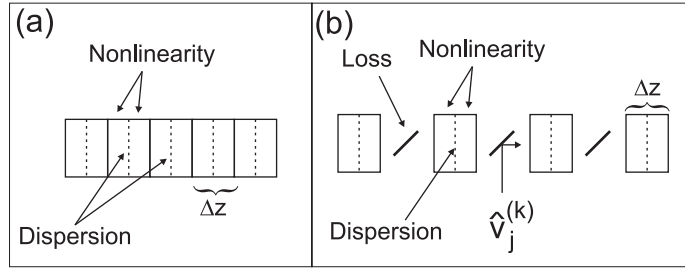


Fig. 2. (a) Schematic model of symmetric split-step Fourier propagation in a fiber. The fiber is divided in a large number of segments of length  $\Delta z$ . The dispersion is calculated at the midplane of each segment (here indicated with a dashed line). (b) Inclusion of loss is obtained by inserting beamsplitters of reflectivity  $\Gamma \Delta z$  between segments. The beamsplitters couple in modes  $v_j^{(k)}$  that are assumed to be in vacuum state.

$$\hat{u}_j(z) \equiv \sum_{m=1}^M (\mu_{jm}(z) \hat{u}_m(0) + \nu_{jm}^*(z) \hat{u}_m^\dagger(0)), \quad (6)$$

where the matrices  $\mu(z)$  and  $\nu(z)$  describe the evolution of the modes, and their off-diagonal elements represent cross-correlations between the various temporal slices of the pulse that develop due to the dispersion. Equation (6) is valid under the same limits that guarantee the validity of the linearization procedure [22].

By substituting Eq. (6) into the evolution equation (4) one obtains the following set of coupled equations

$$\begin{aligned} \frac{\partial \mu_{jm}}{\partial z} &= 2i|\bar{U}|^2 \mu_{jm} + i\bar{U}^2 \nu_{jm} - \frac{i}{2} \text{FFT}^{-1} [\omega^2 \text{FFT} [\mu_{jm}]], \\ \frac{\partial \nu_{jm}}{\partial z} &= -2i|\bar{U}|^2 \nu_{jm} - i\bar{U}^2 \mu_{jm} + \frac{i}{2} \text{FFT}^{-1} [\omega^2 \text{FFT} [\nu_{jm}]], \end{aligned} \quad (7)$$

where we have introduced the fast Fourier transform FFT to solve the dispersive part of the propagation equation and  $\omega$  is the associated frequency variable. The coupled equations can then be solved using the symmetrized split-step Fourier method.

The simulation of the interferometer shown in Fig. 1 is carried out in three steps. First, we evolve the averaged envelopes of the soliton-like and the auxiliary pulses,  $\bar{U}$  and  $\bar{U}'$ , respectively, through equal lengths of fiber. Then, using these numerical solutions for the averaged envelopes, we propagate the associated noise operators,  $\hat{u}'$  and  $\hat{u}''$ . Finally the two fields are mixed at the output beamsplitter (BS2) and the noise of the field emerging from one port of the interferometer is calculated, assuming the use of a direct-detection scheme. The two modes  $\hat{U}'$  and  $\hat{U}''$  propagating in the two arms of the interferometer can be linearized as in Eq. (2) and then expanded as in Eq. (6). The output mode will be  $\hat{U}''' = \bar{U}''' + \hat{u}'''$ , where

$$\begin{aligned} \bar{U}''' &= \sqrt{R_2} \bar{U}' + \sqrt{T_2} \bar{U}'' e^{i\phi}, \\ \hat{u}''' &= \sqrt{R_2} \hat{u}' + \sqrt{T_2} \hat{u}'' e^{i\phi}. \end{aligned} \quad (8)$$

Here  $T_2$  is the transmittivity of the output beamsplitter (BS2),  $R_2 = 1 - T_2$  is the corresponding reflectivity, and  $\phi$  is the phase difference between the two arms of the interferometer that can be changed at will. The low-frequency spectrum  $\Phi_0$  of the current [19] generated in the photodiode is

$$\begin{aligned}
\Phi_0 &\propto \sum_{j,m=1}^M \left\langle \left( \hat{U}_j^{\prime\prime\prime\dagger} \hat{U}_j^{\prime\prime\prime} - |\bar{U}^{\prime\prime\prime}|^2 \right) \left( \hat{U}_m^{\prime\prime\prime\dagger} \hat{U}_m^{\prime\prime\prime} - |\bar{U}^{\prime\prime\prime}|^2 \right) \right\rangle \\
&\simeq R_2 \sum_{m=1}^M \left| \sum_{j=1}^M |\bar{U}_j^{\prime\prime\prime}| \left( \mu'_{jm} e^{-i\theta_j} + \nu'_{jm} e^{i\theta_j} \right) \right|^2 \\
&+ T_2 \sum_{m=1}^M \left| \sum_{j=1}^M |\bar{U}_j^{\prime\prime\prime}| \left( \mu''_{jm} e^{-i\theta_j} + \nu''_{jm} e^{i\theta_j} \right) \right|^2, \tag{9}
\end{aligned}$$

where  $\theta_j = \arg(\bar{U}_j^{\prime\prime\prime})$ , and we have introduced the evolution matrices  $\mu'_{jk}$ ,  $\nu'_{jk}$ ,  $\mu''_{jk}$ , and  $\nu''_{jk}$  for the modes  $\hat{u}'$  and  $\hat{u}''$  similar to those defined in Eq. (6). To evaluate the average in Eq. (9) we have assumed that the modes are initially in the vacuum state. This assumption is valid because in our experiment the measurements of photocurrent fluctuations are made in a frequency band where the laser source is shot-noise limited. The quantum-noise reduction (QNR) is then calculated as the ratio of the output photocurrent fluctuations as normalized to the shot noise [19]

$$\text{QNR} = \frac{\Phi_0|_{(\mu', \mu'', \nu', \nu'')}}{\Phi_0|_{(\mu'_{jm} = \mu''_{jm} = \delta_{jm}, \nu'_{jm} = \nu''_{jm} = 0)}}. \tag{10}$$

Note that the QNR is a function of  $\phi$  [through the dependence of  $\theta_j$  on  $\phi$  in Eqs. (8) and (9)] and can be minimized with respect to this parameter.

### 3 Numerical Analysis: Lossy Fiber

As losses lead to degradation of the QNR, it is important to quantify their effect in order to compare the QNR obtainable in MF with that in standard PM fibers. In this section we study the effect of distributed losses on the propagation of quantum noise in an optical fiber. To do this we need to first include losses in the classical NLSE, Eq. (3), which can be done in a straightforward way

$$\frac{\partial \bar{U}}{\partial z} = \left( i |\bar{U}|^2 - \Gamma \right) \bar{U} + \frac{i}{2} \frac{\partial^2 \bar{U}}{\partial t^2}, \tag{11}$$

where  $\Gamma$  is the loss coefficient [21]. Including losses in the propagation of quantum noise requires coupling of the mode described by  $\hat{U}$  with a reservoir of loss oscillators [23]. To evaluate the effect of this coupling on the overall evolution of the quantum noise in the fiber we introduce an approximate model schematically shown in Fig. 2(b). The fiber is divided into  $P$  segments, where each segment is approximated by a piece of lossless fiber of length  $\Delta z$  followed by a beamsplitter. Propagation of noise through the lossless-fiber segment is described by Eq. (4), while the beamsplitter is introduced to account for the attenuation and the noise (including the back action of losses) accumulated in propagation through the segment. The  $k$ -th beamsplitter has the twofold effect of attenuating the field transmitted by the  $k$ -th lossless fiber segment and coupling in the noise through the modes  $\hat{v}_j^{(k)}$  (one for each temporal slice denoted by the index  $j$ ), which we will assume to be in the vacuum state. Equation (6) can be generalized to the lossy case as

$$\hat{u}_j(z) \equiv \sum_{m=1}^M \left( \mu_{jm}^{(L)}(z) \hat{u}_m(0) + \nu_{jm}^{(L)*}(z) \hat{u}_m^\dagger(0) \right) + \Gamma \Delta z \sum_{k=1}^P \left( \sum_{m=1}^M \left( \xi_{jm}^{(k)} \hat{v}_m^{(k)} + \eta_{jm}^{(k)*} \hat{v}_m^{(k)\dagger} \right) \right), \quad (12)$$

where the effect of attenuation due to the beamsplitters has been included in the propagation matrices  $\mu^{(L)}$  and  $\nu^{(L)}$  by multiplying the matrices resulting from lossless propagation in the  $k$ -th segment by the factor  $(1 - \Gamma \Delta z)$ . The  $\Gamma \Delta z$  factor on the second term in the right-hand side accounts for the back coupling of the beamsplitters. The propagation of the matrices  $\xi^{(k)}$  and  $\eta^{(k)}$  obey the same evolution equations as the matrices  $\mu^{(L)}$  and  $\nu^{(L)}$ , with the proviso that they propagate only through  $P - k$  segments of the fiber. The photocurrent spectral density can be rewritten as

$$\begin{aligned} \Phi_0 \propto & R_2 \sum_{m=1}^M \left| \sum_{j=1}^M \left| \bar{U}_j''' \right| \left( \mu'_{jm} e^{-i\theta_j} + \nu'_{jm} e^{i\theta_j} \right) \right|^2 \\ & + R_2 (\Gamma \Delta z)^2 \sum_{k=1}^P \sum_{m=1}^M \left| \sum_{j=1}^M \left| \bar{U}_j''' \right| \left( \xi'_{jm} e^{-i\theta_j} + \eta'_{jm} e^{i\theta_j} \right) \right|^2 \\ & + T_2 \sum_{m=1}^M \left| \sum_{j=1}^M \left| \bar{U}_j''' \right| \left( \mu''_{jm} e^{-i\theta_j} + \nu''_{jm} e^{i\theta_j} \right) \right|^2 \\ & + T_2 (\Gamma \Delta z)^2 \sum_{k=1}^P \sum_{m=1}^M \left| \sum_{j=1}^M \left| \bar{U}_j''' \right| \left( \xi''_{jm} e^{-i\theta_j} + \eta''_{jm} e^{i\theta_j} \right) \right|^2, \quad (13) \end{aligned}$$

where we have introduced the matrices of evolution for the two arms of the Mach-Zehnder interferometer as in Eqs. (8) and (9) in the previous section.

The numerical solution for propagation of the quantum noise in presence of the distributed losses is not different, in principle, from that in the lossless case, but it requires more computational resources. In Fig. 3 we report a plot of the QNR as a function of the fiber transmittivity  $\eta$ . The propagation length is  $L = 4.3$  soliton periods, the initial strong-pulse energy is that of a fundamental soliton, and the splitting ratio of BS1 is chosen to be 10% and that of BS2 to be 3.5% (i.e.,  $T_1 = 0.1$  and  $T_2 = 0.035$ ). For comparison we have also included a plot of the effect that the same amount of total losses have on the QNR when the propagation in the fiber is lossless but the losses are lumped at the output of the interferometer. From the two curves in Fig. 3 it is evident that the degradation in QNR introduced by the distributed losses is always less than that caused by equal amount of lumped losses placed at the output of the interferometer. This result is consistent with that obtained via an analytical calculation in the case of squeezed-state generation by means of degenerate four-wave mixing [24].

#### 4 Experimental Setup

A schematic of our experimental realization of the Mach-Zehnder interferometer is shown in Fig. 4. The Mach-Zehnder is formed as a polarization interferometer between the two polarization beamsplitters PBS2 and PBS3; each arm including one of the two orthogonal polarization modes of a PM fiber. The light source is a tunable optical-parametric oscillator (Coherent Inc., model Mira-OPO) emitting a train of pulses at a wavelength of approximately 1550 nm with a 75 MHz repetition rate and 200 fs (FWHM) pulse width.

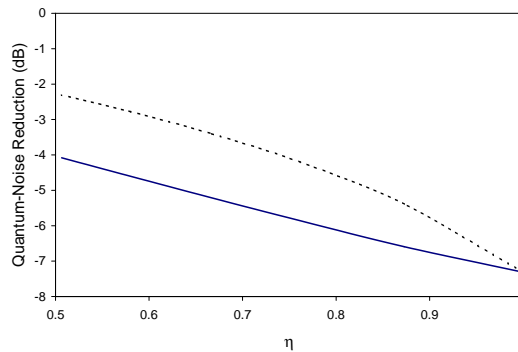


Fig. 3. Plot of QNR versus fiber transmittivity in case of distributed losses (continuous curve) and lumped losses (dashed curve). Propagation distance in the fiber is 4.3 soliton periods,  $T_1 = 0.1$ , the strong-pulse arm is injected with a fundamental soliton, and  $T_2 = 0.035$ .

The pulses are *sech* shaped and nearly Fourier transform limited (time-bandwidth product  $\simeq 0.4$ ). We inject one arm of the interferometer with a strong pulse, propagating in the soliton regime, and the other with a weak, auxiliary pulse propagating in the dispersive regime. The total injected power and the input splitting ratio  $T_1$  of the interferometer are controlled by rotating a half-wave plate (HWP1) and a polarizing beam-splitter (PBS1). Since the pulses propagate with significantly different group velocities in the two polarization modes of the fiber, they are launched delayed with respect to each other so that they overlap at the fiber output. The relative delay is introduced by adding separate free-space propagation paths [*s*(*p*)-polarization reflects from M1 (M2)] for the two polarization modes in the interferometer. This arrangement also minimizes interaction between the two pulses, as they are temporally separated during most of the propagation distance in the fiber. In addition, a piezoelectric control on M1 allows fine tuning of the relative phase between the two pulses. A half-wave plate (HWP2) and a quarter-wave plate (QWP3) are used to inject the *s* and *p* polarized pulses from free space into the correct polarization modes of the fiber. At the output of the fiber, the two pulses are recombined using a half-wave plate (HWP3) and a polarizing beamsplitter (PBS3), which allows us to easily change the output splitting ratio  $T_2$  by turning HWP3. The combined pulse, reflected by PBS3, is reflected off another polarization beamsplitter (PBS4) in order to insure a high polarization purity while minimizing optical losses. The emerging pulse train is then analyzed for its noise characteristics with use of a balanced direct-detection apparatus.

A sample of the experimental results is shown in Fig. 5. In Fig. 5(a) we show a plot of the QNR obtained in a piece of standard PM fiber as a function of the strong-pulse energy. The fiber length was equivalent to 4.3 soliton periods. The plotted QNR has been corrected for the detection efficiency, i.e., the linear losses from the output of the fiber to the detection apparatus, including the fiber's end-face reflectivity and the quantum efficiency of the photodiodes. In 5(b) we show a plot of the QNR, similarly corrected for the detection efficiency, in a piece of MF as a function of the strong-pulse energy. The fiber length was equivalent to 5.9 soliton periods in this case. We observed a maximum QNR of  $6.3 \pm 0.6$  dB in the standard PM fiber and  $4.0 \pm 0.4$  dB in the MF after correcting for the detection efficiencies of 82% and 78%, respectively, in the two cases.

In Fig. 5 we also compare the results of our simulations with the experimental data. In Fig. 5(a) the data taken with the PM fiber are compared with simulations in the lossless case [using the results of Section 2], whereas the data in Fig. 5(b), that pertain

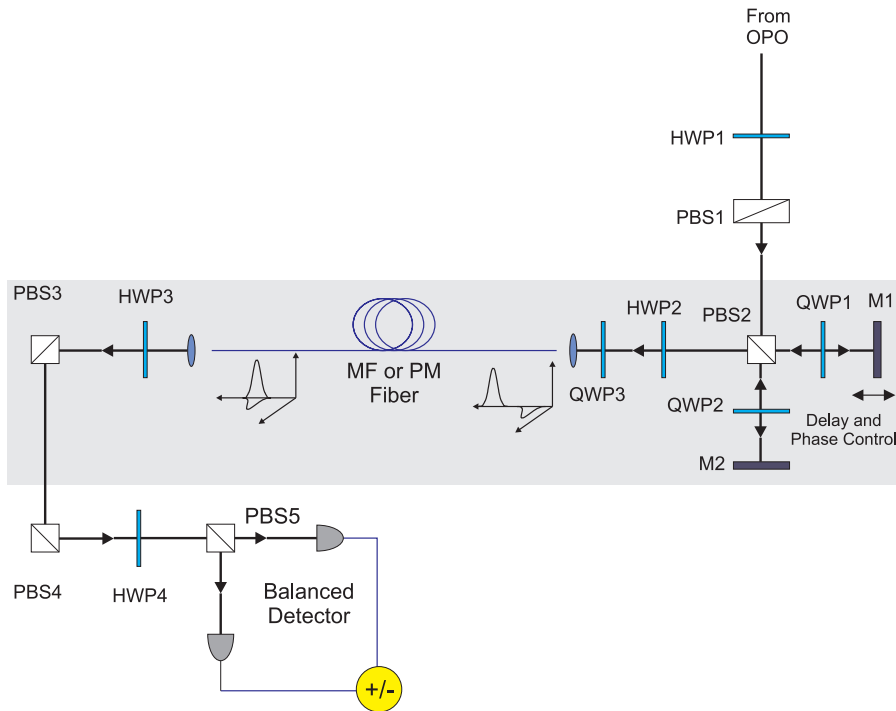


Fig. 4. A schematic of our experimental setup. The shaded area highlights the components that form the Mach-Zehnder polarization interferometer. OPO, optical-parametric oscillator; HWP, half-wave plate; QWP, quarter-wave plate; PBS, polarizing beamsplitter; M, mirror.

to the MF, are compared with simulations including the distributed losses [using the results of Section 3]. We attribute the oscillations in the calculated QNR in both cases to the interference between the quantum noises of the strong and auxiliary pulses. The calculated values of the QNR do not quantitatively agree with the experimental data, which show little evidence of the oscillations. The theory predicts saturation of the detected QNR for large values of  $N^2$  in the case of PM fiber, which we attribute to an increasing temporal mismatch in the overlap between the soliton-like and the auxiliary pulses. We also point out that the lower QNR observed in the MF case cannot be explained by taking into account exclusively the distributed losses in the fiber.

Reasons for the discrepancy between the theory and the experiment, in the lossless case, have been discussed in the literature with authors reaching differing conclusions. Some [6] believe the discrepancy is due to the Raman effect (that we have found to be significant in our setup) and their claim is partially supported by papers that discuss limits on squeezing imposed by the Raman noise [25]. Other authors [26] have reported results of numerical calculations with inclusion of the Raman effect, but the results show that the Raman noise does not seem to play a significant role. Finally, the authors of one experimental paper [2] cooled the fiber to liquid nitrogen temperature and observed an increase in the noise reduction, thus suggesting a preminent role for the phase noise owing to guided-acoustic-wave Brillouin scattering (GAWBS); whereas others [27] were able to achieve a good matching between the theory and the data in an experiment where both GWABS and Raman scattering were negligible.

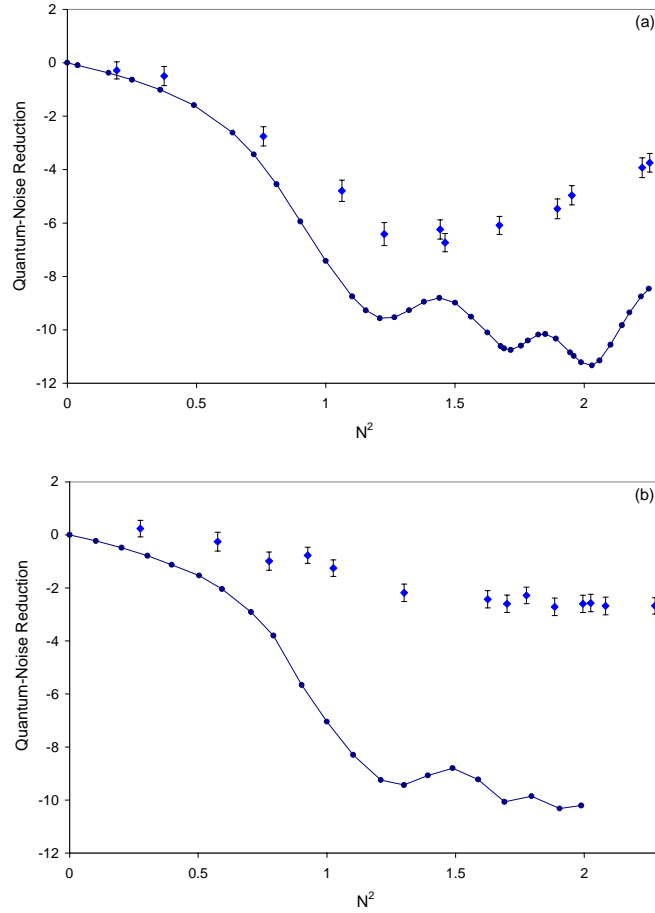


Fig. 5. Plots of QNR corrected for detection losses in the PM-fiber (a) and MF (b) as a function of the energy of the strong pulse expressed in terms of squared soliton-number  $N^2$ . The experimental data (diamonds) are compared with numerical simulations (circles). (a) PM fiber,  $L = 4.3$  soliton periods,  $T_1 = 0.1$ ,  $T_2 = 0.032$ ; (b) MF,  $L = 5.9$  soliton periods,  $T_1 = 0.095$ ,  $T_2 = 0.037$ ,  $\Gamma = 0.01$ . The numerical simulation in (b) is limited to the maximum value of  $N^2$  by the computational resources at our disposal.

## 5 Conclusions

We have presented an analysis of a Mach-Zehnder nonlinear-fiber interferometer that generates amplitude-squeezed pulses of light. A numerical simulation of the linearized NLSE was used to check our understanding of the main processes underlying QNR. Distributed losses in the nonlinear fiber are taken into account to adequately model the MF, in which such losses are not negligible. Although there is a qualitative agreement between the simulation results and the experimental data, the two differ quantitatively in a significant way. We believe that the inclusion of higher-order effects, such as Raman self-frequency shift, cubic dispersion, and third-harmonic generation, is essential for an adequate description of the squeezing process in optical fibers.

The authors thank R. Windeler of Bell Laboratories for providing the MF fiber used in the experiments, G. Biondini for useful discussion on the numerical simulations and E. Corndorf for his help with the computers. This work was supported in part by the U.S. Army Research Office through the MURI grant (DAAD19-00-1-0177) and the associated MURI grant (DAAD19-00-1-0469) for J. E. Sharping.